Dynamic Track Support Loading from Heavier and Faster Train Sets

G. P. RAYMOND AND Z. CAI

The growing use of heavier axle loads and faster speeds in railway train operations increases the likelihood of a track support overloading. Using an analytical dynamic wheel/rail and track interaction model, the effects of heavier axle loads and faster speeds on the increase of wheel/rail forces, rail seat loads, and ballast/subgrade pressures are investigated. The axle loads input include those of typical 50-, 70-, 100-, and 125-ton cars complete with unsprung masses. Also included is a projection of what might be expected in the future should 150-ton cars become acceptable. The dynamic loads estimated are for a track composed of RE 136 rail (having a mass of 68.7 kg/m) supported by CN 55A concrete ties at 610 mm center to center and insulated with EVA tie pads and traversed by a truck with the front wheel having a rounded flat (50-mm length × 0.4-mm depth) and a perfectly shaped rear wheel. The theory and concepts are easily extended to dipped rail joints, rail corrugations, random worn wheels of any profile, and other rail or wheel irregularities traversing wood or concrete tie track.

One of the principal functions of the wheelset is to transfer train loads to the rail track, which in turn transmits and attenuates the loads from the wheels to the ballast and subgrade. With the growing use of heavier train loads and faster speeds, the dynamic wheel/rail forces and track responses associated with wheel, rail, and track irregularities, on present-day (1992) main line tracks, are mostly of high frequency and high magnitude. This will inevitably bring increased deterioration of the track support including the ballast layer and subgrade. Costly damages inflicted on the track components and the wheelset have led to widespread interest in investigating the wheel/rail impact forces. Representative studies included research carried out by Battelle Columbus Laboratories (*1–5*), British Rail Research Division (*6–9*), Track Laboratory of Japan National Railways (*10–12*), and Cambridge University Engineering Department in collaboration with British Rail (*13–15*). All these studies included both analytical and experimental techniques. Most of the studies limit consideration of rail seat and ballast loadings, and the effects on the rail seat loads and ballast pressures resulting from increased axle loads and faster speeds are rarely a subject of focus.

The work reported here is from continuing research on rail vehicle and track dynamics (*16–18*). The primary objective of this research has been the establishment of an improved theoretical model for investigating wheel/rail impact forces and track responses due to wheel and rail irregularities. The effects of a rounded wheel flat loading on typical North American infrastructure are investigated using the model. Rail support loadings from freight cars of different capacity are given particular attention.

Department of Civil Engineering, Queen's University at Kingston, Kingston, Ontario, Canada K7L 3N6.

WHEELSET MODEL

The wheelset is a four-degree-of-freedom lumped mass model as shown in Figure 1. The track model was initially developed for transversely symmetric vibration (*16*). This limits the wheelset model to include only the two unsprung masses (m_u) and the side frame (m_s, I_s) pertaining to one rail. The side frame mass is connected to the unsprung masses through the primary suspension springs at each end (k_1, c_1). The vehicle components above the truck body will not contribute much to high frequency wheel/rail impact because of the low resonant frequencies (below 5 Hz) involved. For this reason, they are ignored here. Only the static car body weight (P_s) is included. The wheel/rail reaction forces on the two wheels are $f_1(t)$ and $f_2(t)$. The equations of motion of the wheelset system are as follows:

$$[M]\{\ddot{Y}\} + [C]\{\dot{Y}\} + [K]\{Y\} = \{f\} \tag{1}$$

where

$$[M] = \begin{bmatrix} m_u & 0 & 0 & 0 \\ 0 & m_u & 0 & 0 \\ 0 & 0 & \frac{m_s}{2} & \frac{m_s}{2} \\ 0 & 0 & \frac{I_s}{l_w} & \frac{-I_s}{l_w} \end{bmatrix} \tag{1a}$$

and

$$[C] = \begin{bmatrix} c_1 & 0 & -c_1 & 0 \\ 0 & c_1 & 0 & -c_1 \\ -c_1 & -c_1 & c_1 & c_1 \\ \frac{-c_1 l_w}{2} & \frac{c_1 l_w}{2} & \frac{c_1 l_w}{2} & \frac{-c_1 l_w}{2} \end{bmatrix} \tag{1b}$$

in which the symbols are as shown in Figure 1. $[K]$ bears the same form as $[C]$ with c_1 in Equation 1b replaced by k_1. The displacement vector $\{Y\} = \{y_1, y_2, y_3, y_4\}^T$ and the force vector $\{f(t)\} = [-f_1(t), -f_2(t), P_s, 0]^T$.

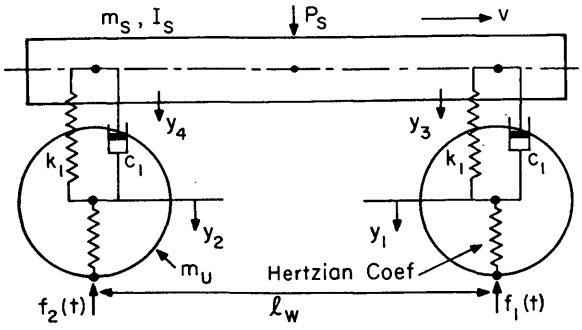

FIGURE 1 Wheelset model.

TRACK MODEL

By a procedure similar to but modified from that developed elsewhere (*7–9*), the track model was formulated by representing the rail and the ties as elastic beams, the rail pads (for a concrete-tie track) as linear springs with viscous damping, and the stiffness and vibration absorbing effect of the underlying track bed as a continuous array of linear springs and viscous dashpots. This is shown in Figure 2. The rail is assumed to have a finite length with the ends clamped and to be supported discretely on the tie beams at the rail seats. The effects resulting from the assumption of a finite length on the wheelset and track responses will be minimal at the midregion away from the ends when the rail length is taken long enough. The current model takes a track length of 40 tie spacings with a single two-axle truck transversing on the rails. Since the behavior and characteristics of the track structure has a great influence on the dynamic interaction between the wheel and the rail and the track support responses, the rail and the ties are described by the more complex and more realistic Timoshenko beam theory. In addition to the flexure and mass inertia considered in the commonly used simple beam theory, the Timoshenko theory takes into account the shear distortion (SD) and the rotatory inertia (RI) effects of the beam. The SD and RI are significant factors in governing high-frequency vibrations of beams.

The equations of the track are obtained by first solving the free vibration of the track and then by applying the method of modal analysis (*16*). The resulting set of equations are

$$\ddot{Q}_n(t) + \sum_{k=1}^{N} 2\xi_{nk}\,\Omega_n\,\dot{Q}_k(t) + \Omega_n^2\,Q_n(t) = f_n(t) \qquad (n = 1, 2, \ldots, N) \qquad (2)$$

where

$Q_n(t)$ = modal time coefficient;
N = number of modes considered;
Ω_n = angular frequency of the track;
ξ_{nk} = coupled modal damping ratio; and
$f_n(t)$ = generalized modal force, expressed by

$$f_n(t) = \frac{1}{M_n}\,[W_n\,(vt)f_1(t) + W_n\,(vt - l_w)f_2(t)] \qquad (3)$$

where

W_n = nth mode shape function of the rail,
M_n = corresponding generalized track mass,
v = train speed, and
l_w = axle spacing.

Equation 2 is a set of N coupled equations. The deflection of the rail is obtained using mode summation:

$$w(x, t) = \sum_{n=1}^{N} W_n\,(x)\,Q_n(t) \qquad (4)$$

HERTZIAN WHEEL/RAIL INTERACTION

The wheel/rail interaction is obtained from the Hertzian contact theory commonly used in wheel/rail contact mechanics and is expressed in the following form:

$$f(t) = G_H[y_W - w(x,t) - \delta(x)]^{\alpha} \qquad (5)$$

where

$f(t)$ = wheel/rail contact force,
y_w = wheel displacement,
$w(x, t)$ = rail deflection at the wheel/rail contact point,
$\delta(x)$ = wheel or rail profile change,
G_H = Hertzian contact coefficient, and
α = constant (1.5 is used here).

By coupling Equations 1 to 5, the wheel/rail interaction forces $f_1(t)$ and $f_2(t)$ and the modal time coefficients $Q_n(t)$ are solved by using the fourth-order Runge-Kutta method with adaptive time stepsize control. The track support responses are then obtained by using the principles of structural dynamics.

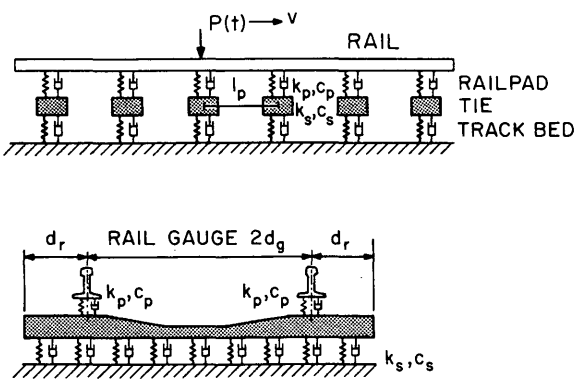

FIGURE 2 Railway track model: *top*, longitudinal track model; *bottom*, cross-tie model.

VALIDATION OF TRACK MODEL

To illustrate the applicability of the finite length track model in studying field rail track vibration problems, the dynamic receptance characteristics of a typical British Rail field track resulting from an earlier study (*16*) is shown in Figure 3.

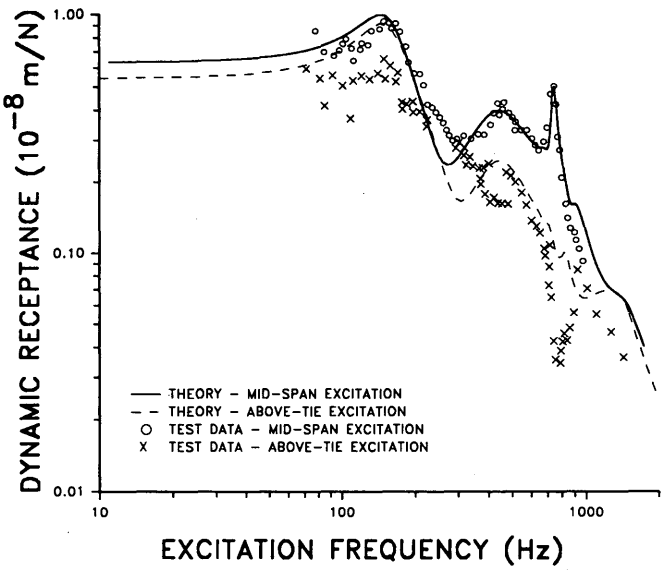

FIGURE 3 Comparison of dynamic receptance of model and field data.

Modal analysis and Fourier transform were used to formulate the theoretical solutions shown in Figure 3. Details of the solution procedure are published elsewhere (*18*). The theoretical results using the Timoshenko beam theory for the rail and the nonuniform tie are compared with field experimental data obtained by Grassie (*15*) for the same track, under both midspan and above-tie excitations. For the midspan excitation, the model gives close agreement to the field measurement data at frequencies below approximately 250 Hz (no data are available below approximately 70 Hz). Above this frequency, the difference between the model and the field data is practically negligible. When the excitation is above a tie, the model solution and field data also compare reasonably well. The response of the track is dominated more by the rail span as a deep beam spanning between two ties when the excitation is at the midspan, and it is dominated more by the rail-pad-tie and ballast system when the excitation is above a tie. The good comparison between the theoretical dynamic receptance results obtained using the finite length track model and the field experiment data indicates that the use of the finite length model is a reasonable representation of the field track under vibration. Further work is under way to validate the model solutions under wheel/rail dynamic interactions. Preliminary results have shown favorable comparison between the theoretical predictions and field measurement data (*19*).

EXAMPLE OF WHEEL/RAIL IMPACT FORCES DUE TO WHEEL FLAT

A typical wheelset with the front wheel having a rounded flat 50 mm long × 0.4 mm deep that is shown in Figure 4 and the rear wheel intact was run across a 40-tie track with concrete ties at various speeds up to 162 km/hr (track and wheel parameters are given in Tables 1 and 2, respectively). The predicted peak impact loads from the wheel flat are shown in Figure 5 for five freight cars of different capacity. The 150-ton car response is a projection of what might be expected should 150 tons become acceptable. The impact load depends highly on the speed. This is particularly so when the train speed is greater than approximately 90 km/hr. The peak load depends to a smaller extent (not shown here) on where the wheel flat strikes the rail, either directly above a tie (above-tie) or between two adjacent ties (midspan). The results presented here are from a wheel flat impact directly above a tie.

The effect of heavier-capacity cars on the peak dynamic wheel/rail loads are clearly seen in Figure 5 over the entire speed range considered. At speeds below approximately 30 km/hr, the increases in the wheel/rail loads from 50- to 150-ton cars are primarily due to the net increase in the static wheel loads. At a higher speed, the dynamic effects of the

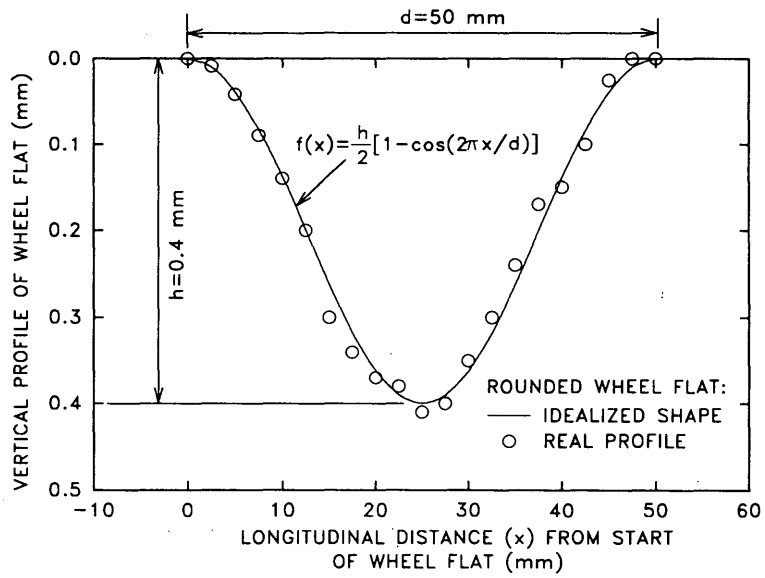

FIGURE 4 Radial wheel flat profile.

TABLE 1 Track Parameters

Tie Parameters (CN 55A Type)		Rail Parameters (RE 136 Type)	
Elastic modulus	E_t= 50 GN/m^2	Elastic modulus	E_r= 207 GN/m^2
Poisson's ratio	= 0.30	Poisson's ratio	= 0.28
Timoshenko shear coeft.	= 0.833	Timoshenko shear coeft.	= 0.34
Tie spacing	= 0.61 m	Cross-sectional area	= 8610 cm^2
Tie length	= 2.50 m	Second moment of area	= 3950 cm^4
Tie width (average)	= 0.25 m	Radius of gyration	= 67.7 mm
Non-uniform section		Bending rigidity	EI_r= 8.18 MN.m^2
Mid-segment length	= 0.90 m	Shear rigidity	κAG_r= 239.3 MN
Mid-segment depth	= 0.14 m	Unit mass	m_r= 68.7 kg/m
End-segment length	= 0.80 m	Rail pad stiffness	k_p= 850 MN/m
End-segment depth	= 0.21 m	Rail pad damping	c_p= 26 kN.s/m
Rail gauge length	= 1.50 m	Track bed stiffness*	k_s= 50 MN/m/m
Tie end to rail seat	= 0.50 m	Track bed damping*	c_s= 34 kN.s/m^2

* These values are assumed to be uniform across the length of the tie.

wheelset and truck side frame masses coupled with the vertical vibration of the track become more prominent. As a result, higher dynamic load increments are induced. A peak wheel/rail load is reached at about 60 km/hr for all the cars, which is followed by a gradual drop in the peak load until 90 km/hr. Above this speed, the wheel/rail impact loads begin to undergo considerable increases with a small increase in the speed. This is more profound for heavier-capacity cars than for lower-capacity ones. For example, the increment between the peak wheel/rail loads of the 125-ton car over the 100-ton car running at 160 km/hr is 3.6 times that between their static wheel loads (or zero speed). This clearly demonstrates that if there exists any irregularity on the wheel (or the rail), which is almost always the case, the use of heavier-capacity cars will certainly engage the rail and the wheelsets to endure dynamic load increments that may be largely in excess of the net increase in the static axle loads.

EXAMPLE OF PEAK RAIL SEAT LOAD AND BALLAST PRESSURE

The corresponding peak dynamic rail seat loads and the peak ballast pressures directly below the rail seat are presented in Figures 6 and 7, respectively, in relation to the speed. The tie for which the rail seat load and the ballast pressure are obtained is the 18th tie of the 40-tie track, above which the wheel flat impact is assumed to occur. Similar to the wheel/rail load shown in Figure 5, the increases in the rail seat loads shown in Figure 6 caused by the net increases in the static wheel loads of the various capacity freight cars are reflected by the initial portions of the curves below 30 km/hr. The sudden increase in the peak rail seat load for all the cars between 30 and 90 km/hr is a direct result of the development of intense dynamic interactions between the wheel and the rail atop the tie, as is indicated in Figure 5 by the quick growth

TABLE 2 Wheel Parameters

Car name (net US ton) Net car weight (MN)	50 0.50	70 0.70	100 1.00	125 1.25	150* 1.50*
Unsprung mass of wheelset (Mg)	1.02	1.10	1.42	1.59	1.79
Mass of side frames (kg)	0.74	0.88	1.13	1.21	1.40
Mass moment of inertia-side frames (kg.m^2)	202	260	363	542	622
Stiffness of primary suspension (MN/m)**	1.50	1.79	2.14	2.80	3.10
Wheel diameter (mm)	762	762	762	965	965
Axle spacing (m)	1.67	1.72	1.78	1.83	1.83
Hertzian coefficient (GN.m$^{-3/2}$)	81.9	81.9	81.9	86.8	86.8
Static wheel load (kN)	94	122	146	178	203

* 150 Ton car data is projected from data on other four cars.
** Damping of primary suspension is assumed to be the same for all the cars at: 9.9 kN.s/m

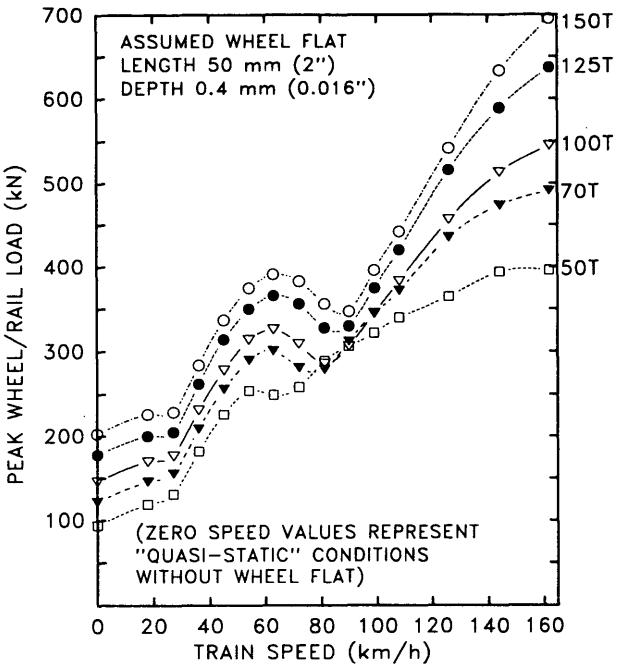

FIGURE 5 Peak wheel impact load due to wheel flat for freight cars of various capacities.

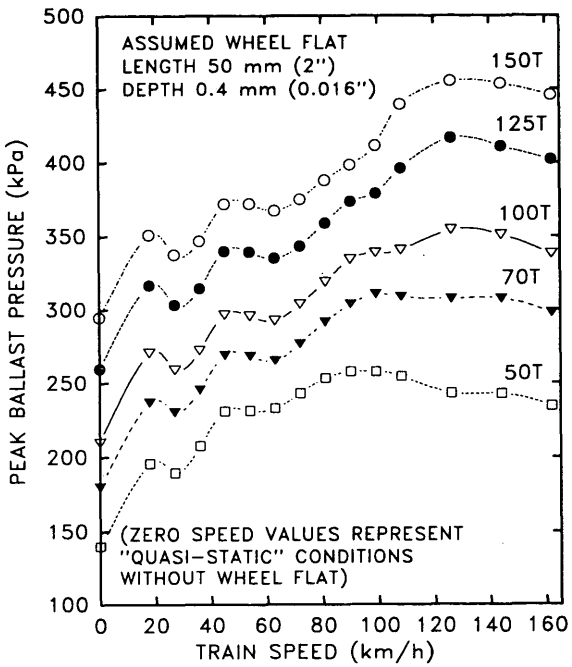

FIGURE 7 Peak ballast pressures for freight cars of various capacities.

of the dynamic peak load within that speed range. Above 90 km/hr, the increase in the peak rail seat load is moderate and begins to flatten for the 125- and 150-ton cars and to gradually decrease for the 100-, 70-, and 50-ton cars.

This leveling off or drop of the rail seat load at higher speeds, despite the marked increase in the wheel/rail impact load shown in Figure 5, is believed to be primarily due to two reasons. One is the shorter duration and thus higher frequency of the wheel/rail impact forces at a faster speed. The other is the increased damping effect of the rail pad, which more effectively attenuates high-speed (or high-frequency) vibrations (*18*). The effect of heavier-capacity cars on the increase of the peak rail seat load is again illustrated by the curves at speeds over approximately 100 km/hr.

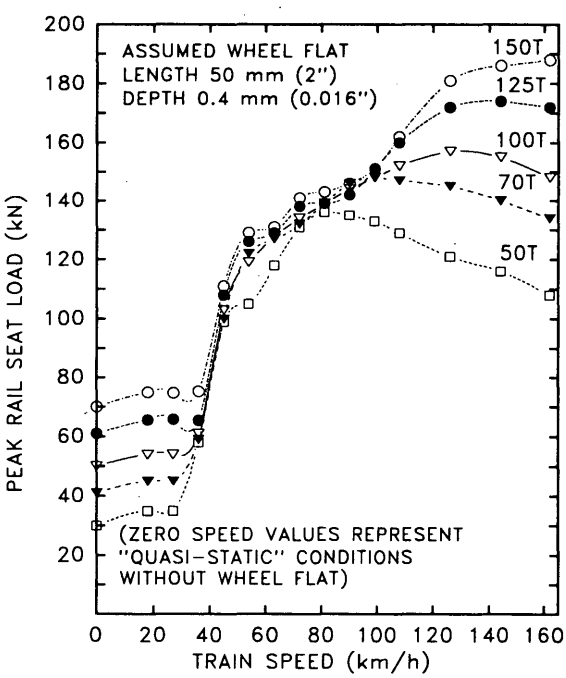

FIGURE 6 Peak rail seat load for freight cars of various capacities.

The effect of an increase in freight car capacity on the increase in the ballast pressure is distinctly evident from Figure 7. The relationship between peak dynamic ballast pressure and speed for different capacity cars, however, is modest compared with the wheel/rail impact forces (Figure 5) and the rail seat loads (Figure 6). For example, the peak ballast pressure under the 125-ton car at 160 km/hr is about 1.5 times its static value, whereas the peak rail seat load is 2.7 times its static value, and the peak wheel/rail load is 3.6 times its static value. Thus, the increase in the ballast pressure due to heavier-capacity cars is to a larger extent attributable to the net increase in the static wheel load than the increase in the wheel/rail load and the rail seat load. This is indicated by the relatively parallel ballast pressure versus speed curves shown in Figure 7. For example, the increment in the peak ballast pressure produced by the 125-ton car over the 100-ton car at 120 km/hr is only 1.3 times the static increment resulting from the net increase in the car weight, whereas the increment gained in the peak wheel/rail load (Figure 5) is close to 2.5 times the net static increment. The relatively moderate relationship between the peak ballast pressure and the speed results from the vibration-attenuating effects of the track structural components, namely the bending rigidity of the rail, the resilience and damping effects of the rail pad, the bending effect of the tie as an elastic beam, and the resilience and damping effects of the ballast itself.

However, below 20 km/hr, the ballast pressure undergoes a higher percentage of increase with the speed than the wheel/

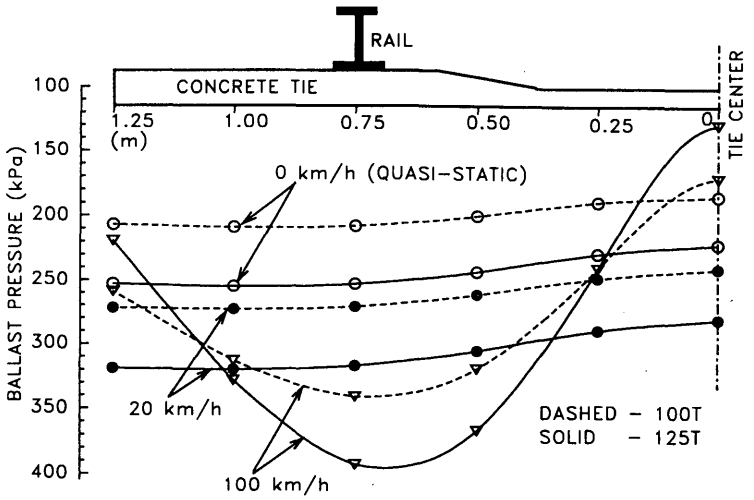

FIGURE 8 Typical distribution of ballast pressures along track tie.

rail load or the rail seat load within the same speed range. The extra increase in the ballast pressure is believed to be introduced by the vertical inertia effects of the concrete tie as a rigid mass on the wheel flat impact. At low speeds, the vertical vibration of the tie is dominated by its rigid mode (75 Hz) as a mass resting on the ballast spring stiffness and damper. At high speeds, the bending mode (155 Hz) of the tie as an elastic beam is more prominent than the rigid mode. This is shown in Figure 8, where the distribution of the ballast pressure along the 18th tie is shown for the 100- and 125-ton cars running at two different speeds as well as under the "quasi-static" condition. These pressure profiles are obtained at the moment when the ballast pressure underneath the rail seat area reaches its peak (the ballast pressure at other points along the tie may be higher than at this moment). The rigid mode and bending mode effects on the ballast pressure distribution are clearly demonstrated by these pressure profiles.

As mentioned earlier, the track structural components, namely the rail, the rail pad, and the tie, absorb a large portion of the dynamic forces generated at the wheel/rail interface. The dynamic impulses created by the wheel flat impact, however, still propagate through the track structures to the ballast/subgrade. Figure 9 shows a typical predicted time history of the ballast pressure under the 18th tie's rail seat area in relation to the front wheel (with flat) travel distance (approximately the middle 10 ties of the 40-tie track) and travel time. When the front wheel flat strikes the rail atop the tie, the ballast pressure oscillates significantly about its quasi-static value as the wheels travel along the rail. Such oscillations in the ballast pressure are harmful to the integrity of the ballast and the subgrade. When the rear intact wheel approaches, the ballast experiences only the quasi-static pressure produced by the static wheel load. The elevation of the ballast pressure due to the increase in the car weight is also evident in the time history traces of the ballast pressure.

CONCLUSIONS

An analytical dynamic wheel/rail and track interaction model and its application in predicting the track support loading

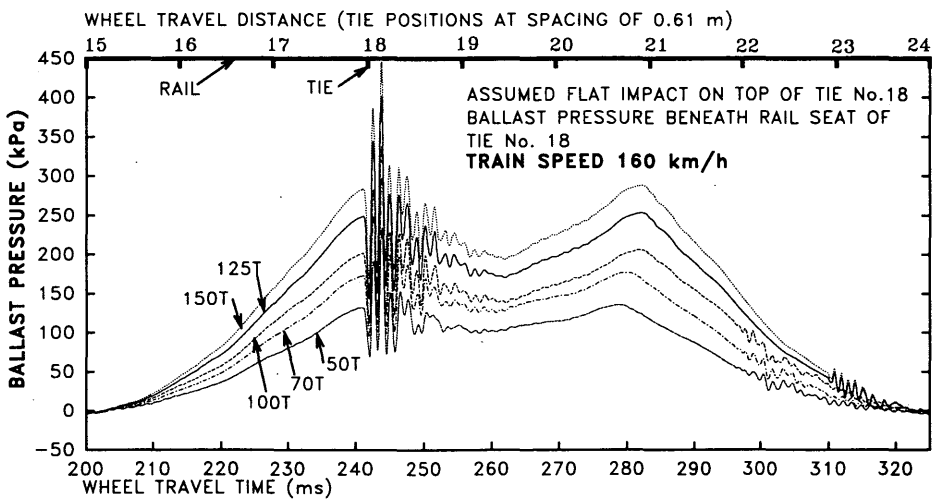

FIGURE 9 Time histories of ballast pressure for freight cars of various capacities.

environment are presented. The dynamic responses of the wheel/rail impact loads, rail seat loads, and ballast pressures produced by a wheel flat on different capacity freight cars commonly in use in North American railway industry are investigated. The theoretical results lead to the following conclusions:

1. For all the freight cars considered, the wheel/rail impact load, the rail seat load, and the ballast pressure depend on the train speed. The effect is largest for the wheel/rail impact load and least for the ballast pressure.
2. The increase in the freight car capacity increases the track support loading. At low speeds, the loading increment is primarily due to the net increase in the car weight. At high speeds, the dynamic interaction between the vehicle masses, mainly those of the truck side frames and the wheelsets, and the track vertical vibration become significant. This causes a loading increment in excess of that gained by the net increase in the static car weight. This effect increases with the speed as well as the capacity of the freight car.
3. The extent to which the loading increment, due to the increase in the car capacity, depends on the speed and car parameters is greatest for the wheel/rail impact load and least for the ballast pressure. For the particular track and train parameters considered, for example, the increment in the wheel/rail impact load from the 100- to the 125-ton car at 100 km/hr is 2.5 times its quasi-static value, whereas the increment in the ballast pressure is 1.3 times its quasi-static value.
4. High-frequency dynamic wheel/rail impact forces propagate into the ballast and subgrade. Thus, the ballast experiences high frequency pressure oscillations, which are adverse to the ballast/subgrade integrity. The ballast pressure distribution across the tie is primarily uniform at low speeds, with the rigid mode of the tie as a mass dominant, and is highly nonuniform at high speeds, with the bending mode of the tie as an elastic beam dominant.

ACKNOWLEDGMENT

Funding by the Natural Sciences and Engineering Council of Canada is acknowledged.

REFERENCES

1. H. C. Meacham and D. R. Ahlbeck. A Computer Study of Dynamic Loads Caused by Vehicle-Track Interaction. ASME Paper 69-RR-1, 1969.
2. D. R. Ahlbeck, H. C. Meacham, and R. H. Prause. The Development of Analytical Models for Railroad Track Dynamics. *Proc., Symposium on Railroad Track Mechanics,* Pergamon Press, 1975, pp. 239–260.
3. D. R. Ahlbeck. An Investigation of Impact Loads due to Wheel Flats and Rail Joints. ASME Paper 80-WA/RT-1, 1980.
4. D. R. Ahlbeck and J. A. Hadden. Measurement and Prediction of Impact Loads from Worn Railroad Wheel and Rail Surface Profiles. *J. Eng. for Ind.,* ASME, Vol. 107, May 1985, pp. 197–205.
5. D. R. Ahlbeck and H. D. Harrison. The Effects of Wheel/Rail Impact Loading due to Wheel Tread Runout Profiles. Paper 6-1. *Proc., 9th Int. Wheelset Congress,* Montreal, Quebec, Canada, Sept. 1988.
6. H. H. Jenkins, J. E. Stephenson, G. A. Clayton, J. W. Morland, and D. Lyon. The Effect of Track and Vehicle Parameters on Wheel/Rail Vertical Dynamic Forces. *Railway Eng. J.,* Jan. 1974, pp. 2–16.
7. S. G. Newton and R. A. Clark. An Investigation into the Dynamic Effects on the Track of Wheelflats on Railway Vehicles. *J. Mech. Eng. Sci.,* Vol. 21, 1979, pp. 287–297.
8. R. A. Clark, P. A. Dean, J. A. Elkins, and S. G. Newton. An Investigation into the Dynamic Effects of Railway Vehicles Running on Corrugated Rails. *J. Mech. Eng. Sci.,* Vol. 24, 1982, pp. 65–76.
9. J. M. Tunna. Wheel-Rail Forces due to Wheel Irregularities. Paper 6-2. *Proc., 9th Int. Wheelset Congress,* Montreal, Quebec, Canada, Sept. 1988.
10. S. Kuroda. Dynamic Variation of Wheel Load Attributed to Vertical Deformation of Rail End. *Q. Rep.,* JNR, Vol. 14, No. 3, 1973, pp. 143–144.
11. M. Hirano. Theoretical Analysis of Variation of Wheel Load. *Q. Rep.,* JNR, Vol. 13, No. 1, 1972, pp. 42–44.
12. Y. Sato. Study on High Frequency Vibrations in Track Operated with High-Speed Trains. *Q. Rep.,* JNR, Vol. 18, No. 13, 1977, pp. 109–114.
13. S. L. Grassie, R. W. Gregory, and K. L. Johnson. The Dynamic Response of Railway Track to High Frequency Vertical Excitation. *J. Mech. Eng. Sci.,* Vol. 24, 1982, pp. 103–111.
14. S. L. Grassie, R. W. Gregory, and K. L. Johnson. The Dynamic Loading of Rails at Corrugated Frequencies. *Proc., Contact Mech. and Wear of Rail/Wheel Systems,* Vancouver, British Columbia, Canada, July 1982, pp. 209–225.
15. S. L. Grassie. Dynamic Modelling of Railway Track and Wheelsets. *Proc., 2nd Int. Conf. on Recent Advances in Struc. Dyn.* (M. Petyt and H. F. Wolfe, eds.), ISVR, University of Southampton, 1984, pp. 681–698.
16. Z. Cai. *Modelling of Rail Track Dynamics and Wheel/Rail Interaction.* Ph.D. thesis. Queen's University at Kingston, Kingston, Ontario, Canada, 1992.
17. Z. Cai and G. P. Raymond. Theoretical Model for Dynamic Wheel/Rail and Track Interaction. *Proc., 10th. Int. Wheelset Cong.,* Sydney, Australia, Sept. 1992, pp. 127–131.
18. Z. Cai and G. P. Raymond. Dynamic Modelling of Parameters Controlling Railway Track Vibration. *Proc., 1st. Int. Conf. Motion and Vibration Control,* Yokohama, Japan, Sept. 1992, pp. 976–981.
19. Z. Cai and G. P. Raymond. Dynamic Wheel/Rail Interaction and Track Responses due to Wheel/Rail Irregularities. Department of Civil Engineering, Queen's University at Kingston, Kingston, Ontario, Canada, 1992.

Publication of this paper sponsored by Committee on Railroad Track Structure System Design.